IJPSR (2024), Volume 15, Issue 9 **(Research Article)**

INTERNATIONAL JOURNAL OF PHARMACEUTICAL SCIENCES AND RESEARCH

Received on 29 March 2024; received in revised form, 10 May 2024; accepted, 06 July 2024; published 01 September 2024

COMPUTATIONAL EXPLORATION OF SMALL MOLECULES AS INHIBITOR TARGETTING CYTOCHROME P4502D6

Sakshi Bhardwaj * and Dhivya Shanmugarajan

Department of Life Sciences, Altem Technologies, Bangalore - 560041, Karnataka, India.

Keywords:

Molecular Docking, CYP2D6, ADMET, TOPKAT, Biovia Discovery Studio, Virtual Screening, Structure-Based Drug Design, Simulation

Correspondence to Author:
Dr. Sakshi Bhardwaj

Application Scientist,
Department of Life Sciences,
Altem Technologies, Bangalore - 560041, Karnataka, India.

E-mail: bhardwajsakshi1@gmail.com

ABSTRACT: Cytochrome P450 2D6 (CYP2D6) is an essential enzyme that affects the safety and effectiveness of a broad range of medications through its metabolism. We provide here an extensive *in-silico* investigation of new drug candidates that target CYP2D6. To find putative CYP2D6 inhibitors, we used virtual screening, structure-based drug design, molecular docking, and simulation approaches in the Biovia Discovery Studio 2022 framework. By maintaining ADMET and TOPKAT filters, a broad variety of small molecules were subjected to virtual screening. After that, the two chosen compounds, cmp1 and cmp13, were used in molecular docking studies against the 4WNU and 4XRZ proteins to evaluate binding affinities and interactions. For 2815 compounds, ADMET and TOPKAT profiling were done to get non-toxic molecules. The non-toxic molecules after filtrations were taken for the docking studies followed by molecular dynamic simulation of the best complex. The best two molecules after ADMET and TOPKAT profiling were taken for docking studies, where these results demonstrated several intriguing therapeutic options with high binding affinities and favorable interactions of compound cmp1 with the active sites of 4WNU proteins, with 26.4705 kcal/mol -CDOCKER energy and 44.37 kcal/mol -CDOCKER interaction energy. These were then selected for molecular dynamic simulations to verify the motion of each atom in the real-time environment. DeltaG_Average = -26.1570 kcal/mol was also computed as the MMPBSA energy. The compound cmp1 was the most significant among the series as aninhibitor TargetingCYP2D6. To demonstrate the same, this molecule needed to be further examined *in-vitro* and *in-vivo*.

INTRODUCTION: According to the science of pharmacogenetics, each patient's genetic profile is considered when creating medicines and customized treatments. As a result, more patients will respond to treatment and fewer will have negative side effects from medications [1].

QUICK RESPONSE CODE

DOI: 10.13040/IJPSR.0975-8232.15(9).2755-72

This article can be accessed online on www.ijpsr.com

DOI link: https://doi.org/10.13040/IJPSR.0975-8232.15(9).2755-72

It is crucial to consider these factors during the drug development process because they may help to explain, or perhaps avoid, the discarding of drug candidates if the right genetic causes are found for lack of response or the occurrence of adverse drug reactions (ADRs) [2].

On the level of drug transporters, drug-metabolizing enzymes, drug targets, and other biomarker genes, one may generally imagine significant pharmacogenetic diversity [3, 4]. Numerous medications, particularly lipophilic substances like psychotropics, must be digested before being excreted in urine.

The cytochrome P450s (haemoproteins), the major phase I enzymes, influence drug metabolizing enzymes the most [5-7]. Many endogenous compounds, such as steroid hormones, lipids, and bile acids, as well as xenobiotics, such as prescription drugs, environmental pollutants, and dietary phytochemicals, are metabolized by CYPs during phase I metabolism [3]. Hence, it is presently believed that up to 25% of the medications that are often prescribed in clinics are metabolized by the cytochrome P450 2D6 (CYP2D6) enzyme, which has historical significance for pharmacogenetics [8-9]. Among these, the highly polymorphic CYP2C9, CYP2C19, and CYP2D6 are responsible for around 40% of the human liver's phase I metabolism [3]. Since these enzymes oversee 80% of phase I drug metabolism, CYP plays a crucial function [4]. Drug efficacy or toxicity may result from inhibition or stimulation of CYP2D6 metabolism, which might change the pharmacokinetic profile of the concurrently delivered drug [8].

Additionally, individual variations in drug metabolism are also influenced by the polymorphisms of CYP1A2, CYP2A6, CYP2B6, and CYP2C8. The polymorphism of CYP2D6, which has a significant clinical impact and was the first of the polymorphic P450s to be described at the molecular level, is likely the most widely studied polymorphically expressed drug metabolizing enzyme in humans [10]. CYP2D6 is a polypeptide of 497 amino acids. The enzyme accounts for only a small percentage of all hepatic P450s, but its role in drug metabolism is extensively higher than its relative content [11]. After being identified as the gene causing the altered activity seen with medications like debrisoquine and others, CYP2D6 became the focus of significant research [12].

It soon became clear that CYP2D6 activity was affected by a wide range of polymorphisms in every region of the world [13-14]. In the initially investigated Caucasian groups, some genotypes resulted in a total lack of CYP2D6 activity; however, research in populations of different ethnic origins indicated reduced function and even hyperfunctional CYP2D6 variants [9-10]. The effect that a CYP2D6 polymorphism has on therapy with any of the drugs listed above depends on the metabolizer status that the polymorphism(s) causes in the patient receiving therapy as well as whether the parent drug is active or if CYP2D6 is necessary for it to be metabolized into an active metabolite. If the parent drug is potent, then ultrarapid metabolizers may experience a lack of efficacy while intermediate metabolizers and poor metabolizers may experience difficulties because of plasma concentrations of the drug that are higher than expected [15]. Treatment with CYP2D6 substrates might be challenging due to medication interactions and genetic variability [16-17]. Numerous medications (such as statins) are CYP2D6 inhibitors and combining an inhibitory medication with a CYP2D6 substrate might change the patient's outward appearance [16]. As a result, the field of CYP pharmacogenetics is crucial for both the development of new medications and their use in clinical practice. Genetic variation has a significant impact on the variability of enzyme activity between individuals because the enzyme is the only drug metabolizing CYP that cannot be generated.

The genetic variation of the enzyme has a significant impact on the metabolism and effects of several pharmaceuticals, including neuroleptics, analgesics, antiemetics, and anticancer drugs [18-19]. Codeine, dextromethorphan, metoprolol, and nortriptyline, to name just a few, are among the medications processed by this enzyme. Initially, it was discovered that these medications had markedly different pharmacokinetics and therapeutic effects, which led to the discovery of the CYP2D6 genetic polymorphism [20-22]. Drugs, for instance, thioridazine, debrisoquine, phenformin, and captopril, which demonstrate comparatively limited therapeutic windows, can be difficult when used by 2D6-poor metabolizers [23-24].

Various computational chemistry techniques have been used to study cytochrome P450s during the past few years, focusing on either the P450 proteins themselves, the small compounds that are processed by or inhibit P450s, or a combination of the two. Due to the clinical significance of P450s in the metabolism of xenobiotics and endogenous compounds and the identification of potential drug-drug interactions, computational models that can predict the potential involvement of P450s in the metabolism of endogenous compounds, drugs, or drug candidates are important tools in drug

discovery and development [25-27]. The purpose of this study was to develop a methodology for the search for prospective CYP2D6 inhibitors using various databases. Computational approaches were utilized to increase the likelihood of finding new inhibitors in a shorter period with high validation predictions. In our paper, we detail our attempts to pinpoint the crucial structural prerequisites for inhibiting CYP2D6 and how these prerequisites helped us develop new, powerful inhibitors. To do this, we have used ligand-based pharmacophore modelling techniques, molecular docking, studies of density functional theory, and virtual screening of huge chemical databases for new scaffolds. These methods provide an excellent opportunity to evaluate the theory of a prospective pharmacological action.

MATERIAL AND METHODS:

Selection of Data: The selection of data is a crucial step for identifying possible lead compounds for subsequent therapeutic development in virtual 3D database screening. Database searches typically have an advantage over other De Novo drug design methods since the retrieved or identified compounds may be conveniently accessible for pharmacological screening techniques. For the virtual screening of the compounds, Biovia Discovery Studio 2022's built-in databases were used, which were downloaded from the CHEMBL. A total of 2815 compounds were selected from the sizable database using filters for property, ADMET, toxicity prediction, Lipnski's rule and Veber's rule for their drug-like characteristics. These drugs' agonistic activity was measured in terms of IC50 values as a gauge of their pharmacological potency. Nevertheless, pIC50 values were also computed.

Preparation of ligands: The selected ligand molecules were prepared by using the prepare ligand module of Biovia Discovery Studio 2022 [26], to correct the representation of ligand chemistry in vivo and enumerate several likely configurations by adding hydrogens, calculated 3D coordinates, enumerated ionization states, ionized functional groups, generated tautomers and isomers, duplicates were removed, bad valences were fixed, standardize charges for common groups were assigned and the largest fragment was retained to carry forward by following the CHARMm-based energy minimizer using 2000 steps of the steepest descent and the conjugate gradient method with a gradient of 0.01 kcal/mol RMSD.

Pharmacokinetic and Pharmacodynamic Properties: All the small molecules were optimized with their property using different tools as filters by the property, ADMET (Absorption, Distribution, Metabolism, Excretion, and Toxicity), Lipinski rule (hydrogen bond donor groups- less than 5, molecular weight less than 500, hydrogen bond acceptor less than 10 and an octanol/water partition coefficient (LogP) value of less than 5) and Veber rule (0 or less than 10 rotatable bonds and polar surface area equal to or less than 140) for their drug-like qualities [27, 28].

ADMET predictions include hepatotoxicity [29], human intestinal absorption [30, 31], aqueous solubility [32-33], and plasma protein binding characteristics (PPB) [34-36]. Hit ligands that passed through each of these screening procedures and satisfied the requirements were used for molecular docking. The potential for developing new therapeutic molecules has increased as a result. It would be extremely beneficial to optimize these characteristics early in the drug design phase to reduce ADMET issues later in the development process.

Specifically, blood-brain barrier (BBB), solubility, and absorption standards were concentrated on ADME. Based on the graphical depiction plotted against ADMET AlogP98 vs. ADMET PSA 2D in the best prediction space, which displays a contained level of 95% for BBB and 99% for human intestine absorption, respectively, the results are interpreted. The TOPKAT AMES mutagen city and NTP rodent carcinogenicity were analyzed for the selected candidates [37-39].

Density Functional Theory (DFT) Calculations: The main molecular characteristics of a molecule were determined through DFT calculations. The candidates found in this investigation had their 3D structures optimized using DFT simulations. These structures were then employed in the calculations of the molecular orbitals, specifically the energy gap (E) and the highest occupied molecular orbital (HOMO), as well as the lowest unoccupied molecular orbital (LUMO) [40].

Preparation of Protein: The two targeted protein structures were selected for our studies with PDB id: 4WNU and 4XRZ having quinidine and BASE 1 as in-bound inhibitors respectively. Both the protein structures are x-ray crystallographic structures which were downloaded via an inbuilt open URL tool in Biovia Discovery Studio 2022 [41], from Protein Data Bank (https://www. rcsb.org). The protein structure of 4WNU is a human cytochrome P450 2D6 with quinidine complex whereas 4XRZ is a human cytochrome P450 2D6 BACE1 Inhibitor 6 Complex. The resolution of the 4WNU protein was reported as 2.26 Å [42] whereas for 4XRZ it was 2.40 Å [43]. The length of selected proteins 4WNU and 4XRZ was found to have 467 and 457 amino acids respectively. The protein reports were analyzed using the protein report and analysis tool of the macromolecule module in Biovia Discovery Studio 2022. It was evident from both the protein reports that some water molecules shared some bonding interactions with the protein and its bound inhibitor. Therefore, we preserved all those water molecules that interacted with the protein while allowing the rest to be deleted. The protein structures were prepared using the prepare protein tool which inserted missing atoms in incomplete residues, modelling missing loop regions using an inbuilt Looper algorithm, deleted alternate conformations (disorder), removed waters which were not required, standardized atom names, protonating titratable residues using predicted pKa and CHARMm based minimization tasks were performed.

Binding site Prediction: The identification of druggable pockets or cavities on a target protein is crucial for the creation of innovative approaches in the drug discovery process. Protein surface cavities are commonly referred to as binding sites, which can exhibit a wide range of sizes and shapes, whether they are ligand-bound [44]. Thus, in the context of drug discovery, more precise criteria are required to distinguish between strong binding sites. The shape and size of cavities, in addition to the chemical complementarity between the ligand and the protein atoms, appear to be the primary drivers of protein-ligand interactions that facilitate binding. It has been assumed that they do not model the ability of a detected cavity to bind a drug-like molecule; instead, they presume that a binding site is a cavity or cleft in the receptor surface.Biovia Discovery Studio 2022 has three protocol to predict binding sites. In this present work, we have used the From PDB site records tool under the Receptor-ligand interaction protocol for the identification of binding sites using protein information available in PDB databases. We have chosen our ligand molecules using the same binding pocket as the protein structures we had chosen because they contained inhibitors. The most time-coupled approach is energy-based, to sum up. By energetically mapping favorable regions for binding, they can compute the energy between a probe and the target on a grid [45, 46].

Molecular Docking: Molecular docking is an *in-silico* method for determining the potential ligand binding landscape within a macromolecular protein or receptor's binding site. Hit compounds from the virtual screening using various filters like ADME, toxicity predictions, Lipinski and Verber's rule and pharmacophoric model were subsequently assessed by molecular docking studies to determine the potential binding orientation within the binding pocket of 4WNU and 4XRZ proteins. The docking ligand (CDOCKER) tool of the Receptor-ligand interaction module of Biovia Discovery Studio 2022 [47], was utilized to check the interactions between the proteins and ligands. The CDOCKER algorithm has generated X:6.94255, Y:23.6642, Z:-3.57496 sphere with a radius of 23Å coordinates for the binding site from receptor cavity of 4WNU and X:-5.8635, Y:26.7216, Z:-79.2442 with the radius of 26 Å for 4XRZ protein. The highest binding affinity of the ligand to the receptor protein is provided by a lower value of -CDOCKER energy and -CDOCKER interaction energy. The most stable protein-ligand complexes were then prepared for molecular dynamics (MD) simulations, which could replicate the circumstances of *in-vitro* and *in-vivo* investigations.

Calculate Binding free Energy: The binding free energy [48, 49] of simulated trajectories in Molecular Mechanics-Poisson Boltzmann with non-polar Surface Area (MMPBSA) was computed via the subsequent formula:

$$Gbinding = G(a) – (G(b)+ G(c))$$

Here, Ga, it represents the protein-ligand complex's overall free energy, Gb is the free energy of protein and Gc, is the free energy of the ligand.

One of the most popular techniques for calculating the interaction energy of biomolecular complexes is the MM-PBSA methodology. MM-PBSA can decode large conformational changes and entropic contributions to the binding energy in conjunction with MD simulation.

Molecular Dynamic Simulations: The Standard dynamic cascade (SDC) protocol of Biovia Discovery Studio 2022 was used to perform molecular dynamic simulation of protein-ligand complexes. Before SDC we applied CHARMM force field to the protein and ligand complex followed by their solvation by providing orthorhombic cell shape explicit periodic boundary. Some counterions (Na+, Cl−) were also added to the system during salvation to neutralize the system. The final frames generated in SDC were subjected to Dynamic NAMD for 50 ns on a GPU mode with NPT ensemble and 300K temperature which used the Langevin dynamic algorithm for temperature control and Langevin Piston for pressure control. Once dynamics had been completed the Analysis trajectory tool was used to get the Root mean squared deviation (RMSD), Root mean squared fluctuation (RMSF) and Radius of gyration (Rg).

RESULTS AND DISCUSSION:

Preparation of Compounds: Structurally diverse, 2815 compounds were chosen with their IC50 values from the inbuilt P450_2D6_chembl_database of Biovia Discovery Studio 2022. As a measure of pharmacological potency, the agonistic activity of these compounds was measured in terms of IC50 values, as they were bio-assessed in similar circumstances. However, pIC50 values were also calculated. Initially, various pharmacokinetic, physiochemical and pharmacodynamic filters like ADMET/TOPKAT, Lipinski and Verber's rule were applied for the selection of lead molecules. After, by keeping all the filters for the selection of lead molecules we prepared ligand molecules and enumerated their likely configuration. A detailed description of ADMET and Toxicity profiling of selected molecules is given in **Table 1** and **2**. The ADMET plot between ADMET_AlogP98 and ADMET_PSA_2D is given in **Fig. 1**, to filter out the molecules which were not coming under the selection criteria. Out of 2815 compounds, a list of twenty-five ligand molecules were chosen based on their pharmacokinetic (ADMET solubility level, ADMET_BBB level, ADMET_CYP2D6, ADMET Hepatotoxicity, ADMET absorption level, and ADMET_PPB prediction) and pharmacodynamic (TOPKAT Mouse Female NTP and TOPKAT Ames Mutagenesis) properties were listed in **Table 2**. In conjunction with ligand molecules, quinidine serves as a standard reference molecule. The ligand molecules were further prepared by adding hydrogens using the software's prepare ligand protocol. Their 3D coordinates were then calculated, their ionization states were counted, their functional groups were ionized, tautomers and isomers were produced, duplicates were eliminated, incorrect valences were fixed, charges for common groups were standardized, and the largest fragments were sorted. In Biovia Discovery Studio there are six different methods available for the conformation generation. In the present work, the BEST conformation method was chosen for the generation of conformation, as it works with the best coverage of conformational space. Detailed information about the TOPAKT Ames Mutagenesis and Mouse Female NTP model prediction for selected compounds, is given in **Fig. 3** to **7**, with its top chemical features for positive and negative contribution towards toxicity.

TABLE 1: DETAILED DESCRIPTION OF CRITERIA FOR SELECTION OF 22 LIGAND MOLECULES FROM THE SERIES OF 2860 MOLECULES BASED ON THEIR PHARMACOKINETIC PREDICTIONS (ADMET)

Parameters	Description
Aqueous solubility	Improved bioavailability of drug with solubility (DS predicts at 25° C) Level=3 (Good)
Blood-brain barrier penetration (BBB)	To predict blood/brain conc., drug should cross BBB, hence lipophilic, especially for CNS drugs level=0 (very high), level=1 (high), level=2 (optimal)
Cytochrome P450 (CYP450) 2D6 inhibition	To predict enzyme inhibition, involved in metabolism, primary located in liver and CNS level=False (non-inhibition), True (inhibition)
Hepatotoxicity	To predict liver toxicity level= False (Good), True (Bad)
Human intestinal absorption (HIA)	To predict absorption after oral administration, also predicts polar surface area (PSA), helps in drug transportation, more PSA effects drug penetration into cell

	membrane (LT 140 Å) level= 0 (Good), 1(moderate)
Plasma protein binding	To predict binding of drug to blood plasma protein, binding to PPB affects drug bioavailability, hence effects its efficacy. level= False (Good)

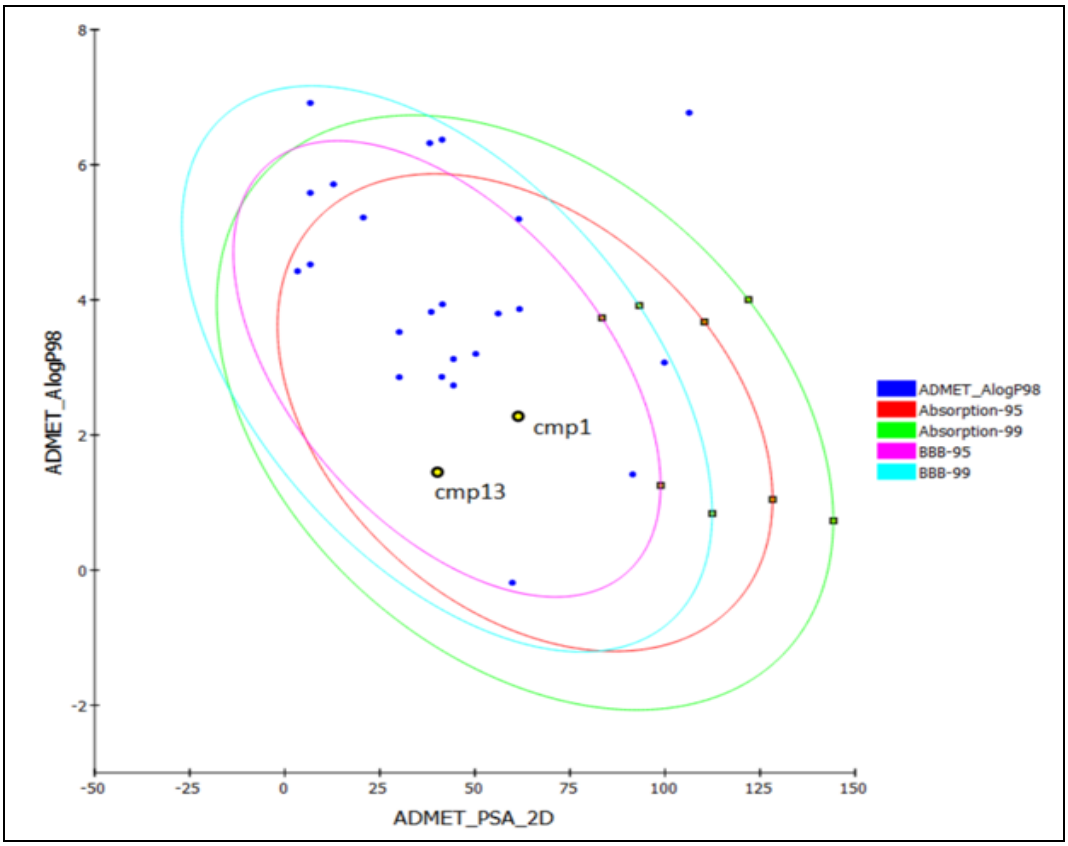

FIG. 1: ADMET PLOT IN BETWEEN ADMET_ALOGP98 AND ADMET_PSA_2D AFTER FILTERING THE LIGAND MOLECULES BASED ON THEIR ADMET PROPERTIES

TABLE 2: A LIST OF SELECTED TWENTY-FIVE LIGAND MOLECULES ON BASIS OF THEIR PHARMACOKINETIC PROPERTIES (ADMET SOLUBILITY LEVEL, ADMET_BBB LEVEL, ADMET CYP2D6, ADMET_HEPATOTOXICITY, ADMET ABSORPTION LEVEL, ADMET PPB PREDICTION) AND PHARMACODYNAMIC PROPERTIES (TOPKAT MOUSE FEMALE NTP AND TOPKAT AMES MUTAGENESIS)

Comp	IC50	ADMET solubility level	ADMT BBB level	ADMET CYP2D6	ADMET Hepato-toxicity	ADMET Absorption level	ADMET PPB prediction	TOPAKT Mouse_ Female NTP	TOPAKT Ames Mutagenesis
cmp1	1	3	2	false	false	0	true	Non-Carcinogen	Non-Mutagen
cmp2	6.3	2	0	true	false	0	true	Non-Carcinogen	Non-Mutagen
cmp3	6.3	2	1	false	false	0	false	Non-Carcinogen	Non-Mutagen
cmp4	7.9	3	3	false	true	0	true	Non-Carcinogen	Non-Mutagen
cmp5	6.3	2	1	false	false	0	true	Non-Carcinogen	Non-Mutagen
cmp6	10	3	2	true	false	0	false	Carcinogen	Non-Mutagen
cmp7	1.6	2	1	true	true	0	true	Non-Carcinogen	Non-Mutagen
cmp8	6.3	3	1	true	false	0	true	Carcinogen	Non-Mutagen
cmp9	6.3	3	3	false	false	0	false	Non-Carcinogen	Non-Mutagen
cmp10	10	2	1	false	true	0	true	Non-Carcinogen	Non-Mutagen
cmp11	7.9	0	0	true	false	2	true	Non-Carcinogen	Non-Mutagen
cmp12	10	2	1	true	false	0	true	Non-Carcinogen	Non-Mutagen
cmp13	1	3	2	false	false	0	false	Carcinogen	Non-Mutagen
cmp14	6.3	1	0	true	false	1	true	Non-Carcinogen	Non-Mutagen
cmp15	4	2	1	false	true	0	false	Non-Carcinogen	Non-Mutagen
cmp17	6.3	1	0	true	true	1	true	Non-Carcinogen	Non-Mutagen
cmp18	6.3	1	4	true	true	2	false	Non-Carcinogen	Non-Mutagen
cmp19	6.3	4	3	false	false	0	false	Non-Carcinogen	Non-Mutagen

cmp20	2.5	2	1	false	true	0	true	Non-Carcinogen	Mutagen
cmp21	12.6	2	0	true	false	0	true	Non-Carcinogen	Non-Mutagen
cmp22	12.6	1	0	false	false	1	true	Non-Carcinogen	Non-Mutagen
cmp23	10	2	0	true	false	1	true	Non-Carcinogen	Non-Mutagen
cmp24	10	1	1	false	true	0	true	Carcinogen	Mutagen
cmp25	10	2	0	true	false	0	true	Non-Carcinogen	Non-Mutagen
quinidine	1.2	3	2	true	false	0	false	Carcinogen	Non-Mutagen

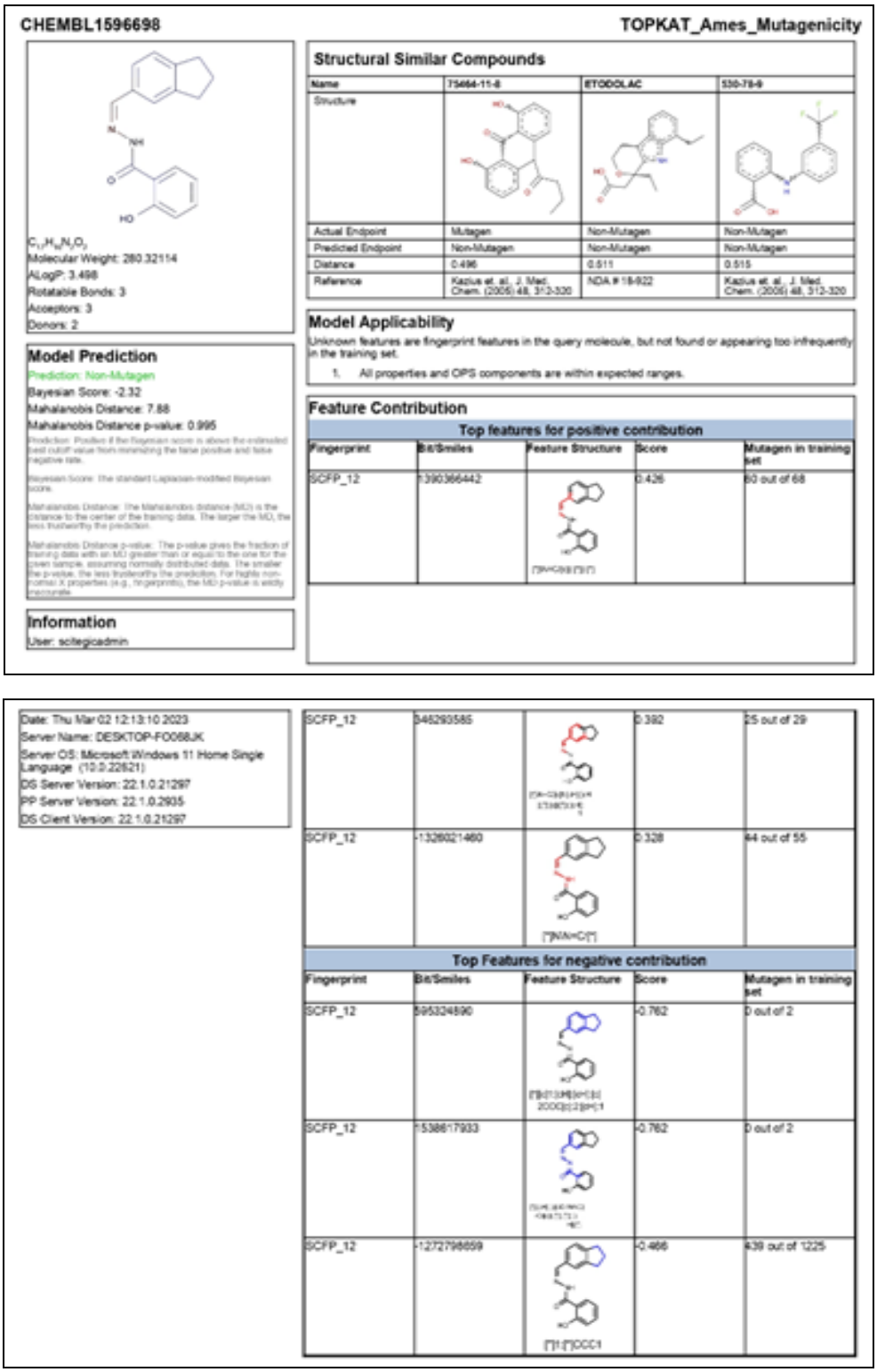

FIG. 2: TOPAKT AMES MUTAGENESIS MODEL PREDICTION FOR CMP1, WITH ITS TOP CHEMICAL FEATURES FOR POSITIVE AND NEGATIVE CONTRIBUTION TOWARDS TOXICITY

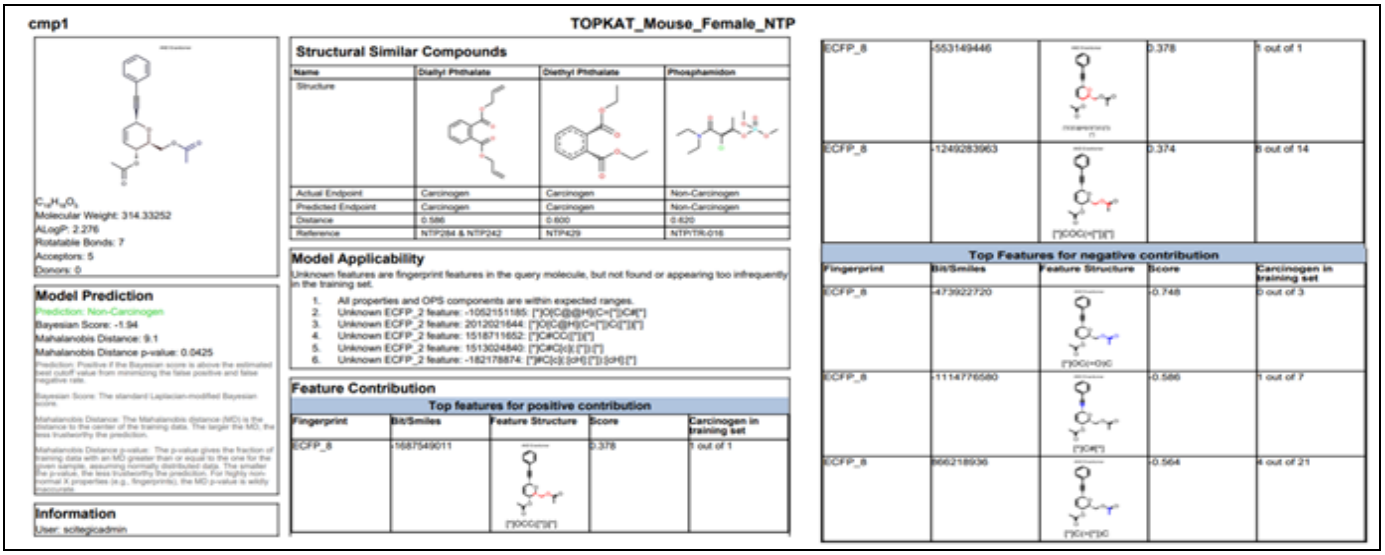

FIG. 3: TOPAKT_MOUSE_FEMALE_NTP MODEL PREDICTION FOR CMP1, WITH ITS TOP CHEMICAL FEATURES FOR A POSITIVE AND NEGATIVE CONTRIBUTION TOWARDS TOXICITY

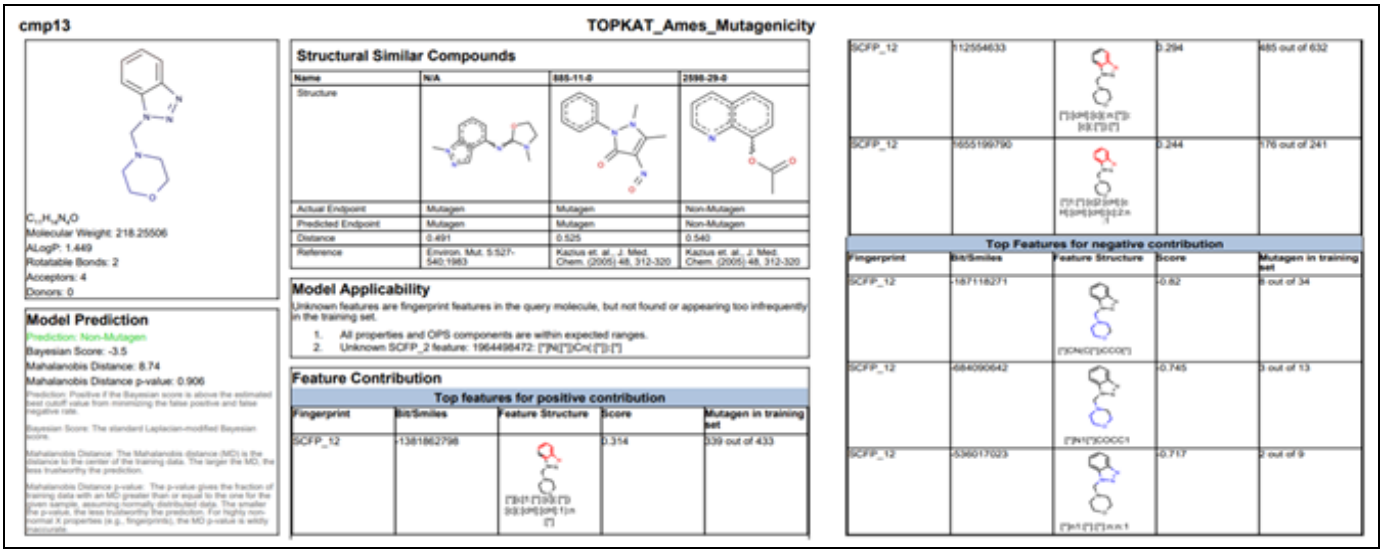

FIG. 4: TOPAKT_AMES MUTAGENESIS MODEL PREDICTION FOR CMP13, WITH ITS TOP CHEMICAL FEATURES FOR POSITIVE AND NEGATIVE CONTRIBUTION TOWARDS TOXICITY

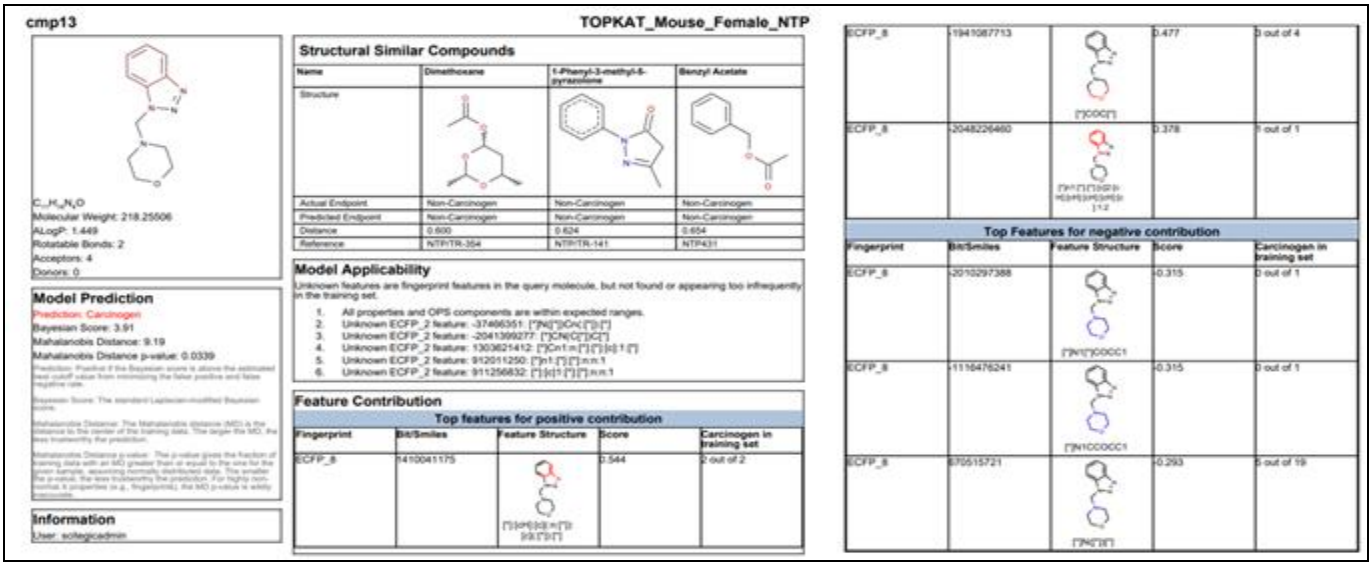

FIG. 5: TOPAKT_ MOUSE_FEMALE_NTP MODEL PREDICTION FOR CMP13, WITH ITS TOP CHEMICAL FEATURES FOR A POSITIVE AND NEGATIVE CONTRIBUTION TOWARDS TOXICITY

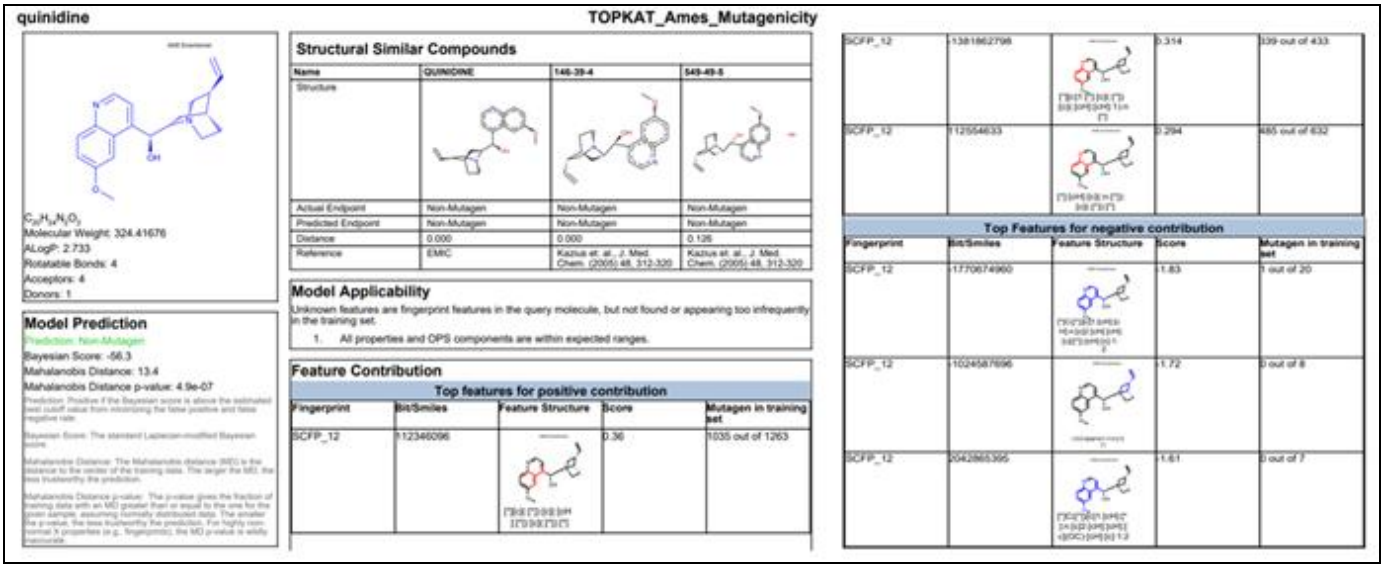

FIG. 6: TOPAKT_ AMES MUTAGENESIS MODEL PREDICTION FOR QUINIDINE, WITH ITS TOP CHEMICAL FEATURES FOR POSITIVE AND NEGATIVE CONTRIBUTION TOWARDS TOXICITY

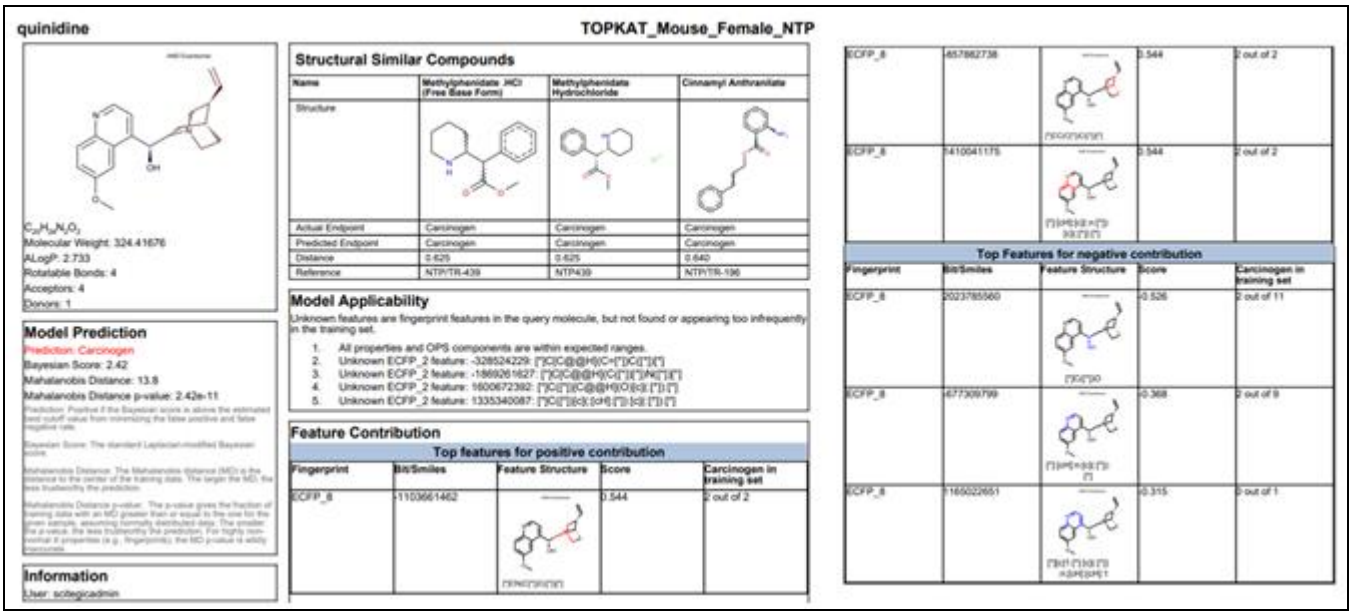

FIG. 7: TOPAKT_ MOUSE_FEMALE_NTP MODEL PREDICTION FOR QUINIDINE, WITH ITS TOP CHEMICAL FEATURES FOR POSITIVE AND NEGATIVE CONTRIBUTION TOWARDS TOXICITY

Preparation of Protein Structure: The selected protein structures were prepared by using protein prepare protocol of Biovia Discovery Studio 2022. First protein structure was analyzed using Protein report and analysistool.

During the protein preparation, the HOH753, HOH767, HOH769, HOH821, HOH822, and HOH887 water molecules for 4WNU and HOH714, HOH720, HOH721, HOH725, HOH752, HOH764 and HOH778 for 4XRZ were retained. The pocket amino acids of 4WNU as ARG101, VAL119, PHE120, TRP128, ARG132, ALA305, GLY306, THR309, THR313, VAL374, HIS376, PHE436, SER437, ARG441, CYS443, LEU444, GLY445 and for 4XRZ as ARG101, VAL119, PHE120, TRP128, ARG132, ILE186, THR309, THR313, GLN364, VAL374, HIS376, LEU399, PRO435, PHE436, SER437, ARG441, CYS443, LEU444, GLY445 were identified. The structures of protein were validated by Ramachandran plot **Fig. 8** showing maximum amino acids into the allowed region. The local backbone conformation of each residue in a protein is graphically depicted by the Ramachandran Plot. In the plot glycine was represented as a triangle, proline as a square, and all other types as a circle.

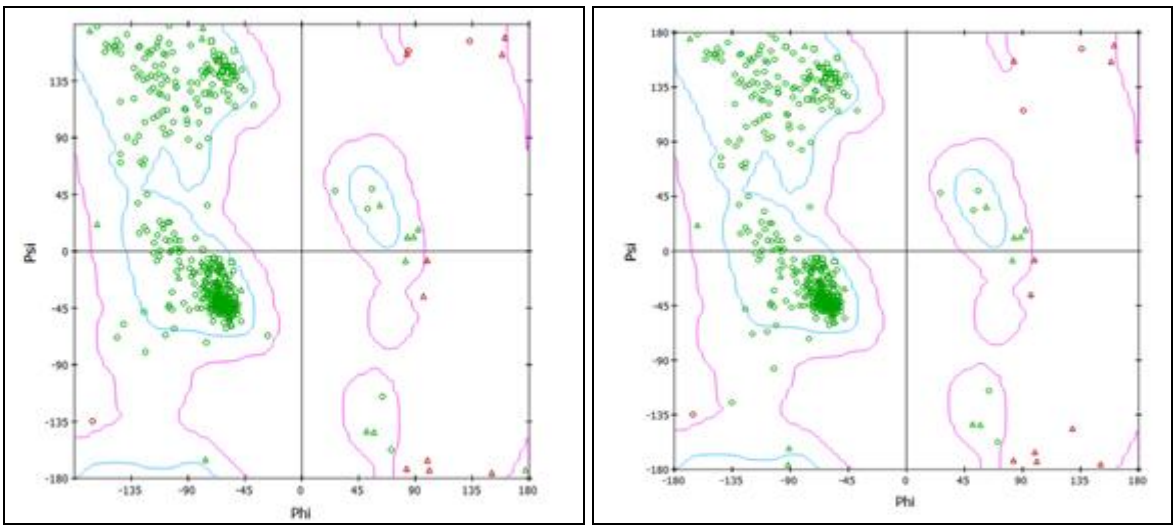

FIG. 8: (A) RAMACHANDRAN PLOT OF PROTEIN 4WNU (B) RAMACHANDRAN PLOT OF PROTEIN 4XRZ

Binding site Prediction: Among three protocols present in Biovia Discovery Studio we have used, from PDB site records tool from Receptor-ligand interaction protocol. The software uses Flood filling algorithm for the generation of binding sites. The X, Y and Z coordinates of the binding site sphere were identified as 5.094727, -2.717602 and 14.032852 respectively. The radius of the binding site sphere was found to be 8.8 Aº. The red sphere of the binding site on both protein structures is shown in **Fig. 9.**

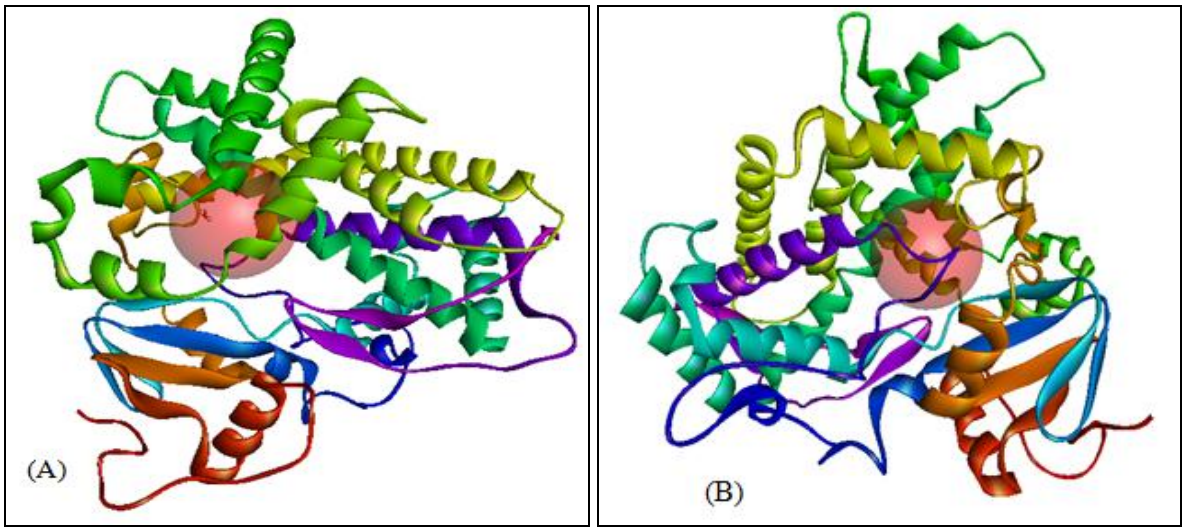

FIG. 9: (A) RED SPHERE SHOWS THE BINDING SITE OF PROTEIN 4WNU (B) RED SPHERE SHOWS THE BINDING SITE OF PROTEIN 4XRZ

Molecular Docking: The present research work has been done via using the CDOCKER protocol of Biovia Discovery Studio 2022 for docking of ligand molecules [50] CDOCKER is a robust CHARMm-based docking technique that has been demonstrated to produce extremely accurate docked poses. Here, high-temperature molecular dynamics is used to create a collection of ligand conformations. The process of translating the ligand's centre to a specific point within the receptor active site, followed by a series of random rotations, results in random orientations of the conformations. Every orientation is put through simulated molecular dynamics annealing. The temperature is raised to a high level and then lowered to the desired level. A final minimization of the ligand in the rigid receptor using non-softened potential is performed. The CHARMm energy (interaction energy plus ligand strain) and the interaction energy alone are determined for each final position. The stances are sorted by CHARMm energy, and only the poses with the

highest scores (more adverse, favoring binding) are kept. CDOCKER can also be used as a docking refinement method if ligands are pre-positioned in the receptor active site (without a site sphere defined). The workflow followed for CDOCKER docking protocol is given in **Fig. 10.**

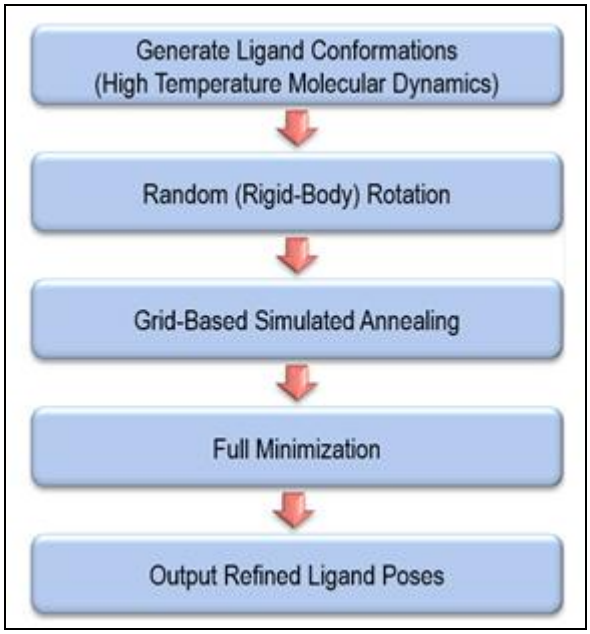

FIG. 10: WORKFLOW FOLLOWED FOR CDOCKER DOCKING PROTOCOL OF BIOVIA DISCOVERY STUDIO

The CDOCKER docking protocol used the Momany-Rone ligand partial charge method. The pose cluster radius was set to 0.1 for the generation of 10 random conformations, with 1000 dynamic steps. The docking summary shown by the software includes the number of refined poses and the ligands which failed to be docked. Docking poses are ordered by -CDOCKER_Energy where a higher value indicates a more favourable binding, this score includes internal ligand strain energy and receptor-ligand interaction energy. The negative of the interaction energy is also reported as -CDOCKER_Interaction_Energy. The top two compounds were designated as the best inhibitors and chosen for additional analysis after they were bound to each target with the highest binding affinity.The docked results for top ligand molecules with their best poses i.e. cmp1 and cmp13 were analysed in terms of -CDOCKER Energy and -CDOCKER Interaction Energy.

The compound cmp1 demonstrated the lowest binding affinity 26.4705 kcal/mol with 4WNU and 23.5713 kcal/mol with 4XRZ in terms of -CDOCKER Energy and 44.37 kcal/mol with 4WNU and 40.691 kcal/mol with 4XRZ in terms of -CDOCKER Interaction Energy which was followed by the compound cmp13, 14.9831 kcal/mol with 4WNU and 12.6244 kcal/mol with 4XRZ in terms of -CDOCKER Energy and 31.9318 kcal/mol with 4WNU and 29.6301 kcal/mol with 4XRZ in terms of -CDOCKER Interaction Energy. As a reference molecule, quinidine hasn't demonstrated particularly strong interactions with any proteins. The -CDOCKER Interaction Energy was 45.9235 kcal/mol with 4XRZ and 44.2938 kcal/mol with 4WNU, while the -CDOCKER Energy for quinidine was determined to be -17.8009 kcal/mol with 4WNU and -12.0632 kcal/mol with 4XRZ. Comparing the compounds cmp1 and cmp13 to the reference quinidine molecule, it was found that the former demonstrated noticeably better binding interactions with the chosen proteins. The -CDOCKER Energy and -CDOCKER interaction Energy for quinidine, cmp1, and cmp13 are shown in **Table 5** and **6**. The docking score and binding interactions of cmp1 have shown the most significant association with the 4WNU as compared with cmp13. The oxygen atom at position ten in compound cmp1 has been shown to form one conventional hydrogen bonding with SER304.

Three other carbon-hydrogen bindings were also shown, one with GLN244 by another oxygen atom at position thirteen, and two with SER304 and oxygen and hydrogen atoms at positions eleven and six respectively. Position sixteen is the aromatic ring's pi alkyl interaction with GEU121. These bonds, especially hydrogen bonds, have a significant impact on the specificity of ligands. Additionally, three interactions between water molecule HOH822 and the oxygen atoms at positions one and eight have been observed. In compound cmp13, there are four carbon hydrogen bonds were identified one in between one hydrogen atom present in seventh position and GLU216, two in between two hydrogen present in second position and SER304 and one in between triazole moiety and LEU213.

A total of four pi alkyl interactions were observed, where two formed in between morpholine ring and PHE483, PHE120, one in between ALA300 and aromatic ring present and one in between triazole

moiety and LEU213. It was also observed that PHE247 and the aromatic ring had one pi-pi interaction. The reference molecule quinidine, on the other hand, has shown one conventional hydrogen bond between hydrogen atom of -OH group and GLU216. One hydrogen bond was seen in the HOH822 and -OH group. Whereas the reference molecule, quinidine, has shown one conventional hydrogen bond in between hydrogen atom of -OH group and GLU216.One hydrogen bond was seen in the HOH822 and -OH group. Additional interactions that were observed involved pi alkyl and different amino acids, such as ALA300, PHE120, PHE483, ALA305, LEU248 and LEU110.Figure 17 provides a detailed graphical description of all the bonding with cmp1, cmp2, and quinidine. In 17a, the compound cmp1 docking position with 4WNU is displayed, and in 17b, the cmp13 docking stance with 4WNU is illustrated, in 17c quinidine docking position with 4WNU is presented, while the interaction diagram of cmp1 with 4WNU is depicted in 17d, in 17e the interaction diagram of cmp13, and the 17f quinidine interaction diagram is illustrated.

It was discovered that certain chemicals' binding interactions with 4XRZ were less substantial than those with 4WNU. It has been discovered that the compound cmp1 interacts pi alkyl with PHE120, ALA305, and LEU248. The compound cmp13 exhibited a single carbon-hydrogen bond between the fifth-position hydrogen and GLU216, as well as between the pi anion and GLU216 and PHE247, LEU213, and ALA305, respectively. On the other hand, quinidine has demonstrated carbon-hydrogen interaction between the hydrogen atom and SER304 and the oxygen atom and LEU213. It has been seen that HOH714 and hydrogen atoms interact. However, interactions with PHE120, ALA305, LEU110, Leu121, and GLY212 were also seen to be pi alkyl, alkyl, and amide pi stacked. **Fig. 18** provides a detailed graphical description of all the bonding with cmp1, cmp2, and quinidine. In 18a, the compound cmp1 docking position with 4XRZ is displayed, and in 18b, the cmp13 docking stance with 4XRZ is illustrated, in 18c quinidine docking position with 4XRZ is presented, while the interaction diagram of cmp1 with 4XRZ is depicted in 18d, in 18e the interaction diagram of cmp13, and the 18f quinidine interaction diagram is illustrated.

TABLE 3: DOCKING RESULTS OF COMPOUNDS CMP1, CMP13 AND QUINIDINE WITH 4WNU

S. no.	Compound	-CDOCKER Energy	-CDOCKER Interaction Energy
1	cmp1	26.4705	44.37
2	cmp13	14.9831	31.9318
3	quinidine	-17.8009	44.2938

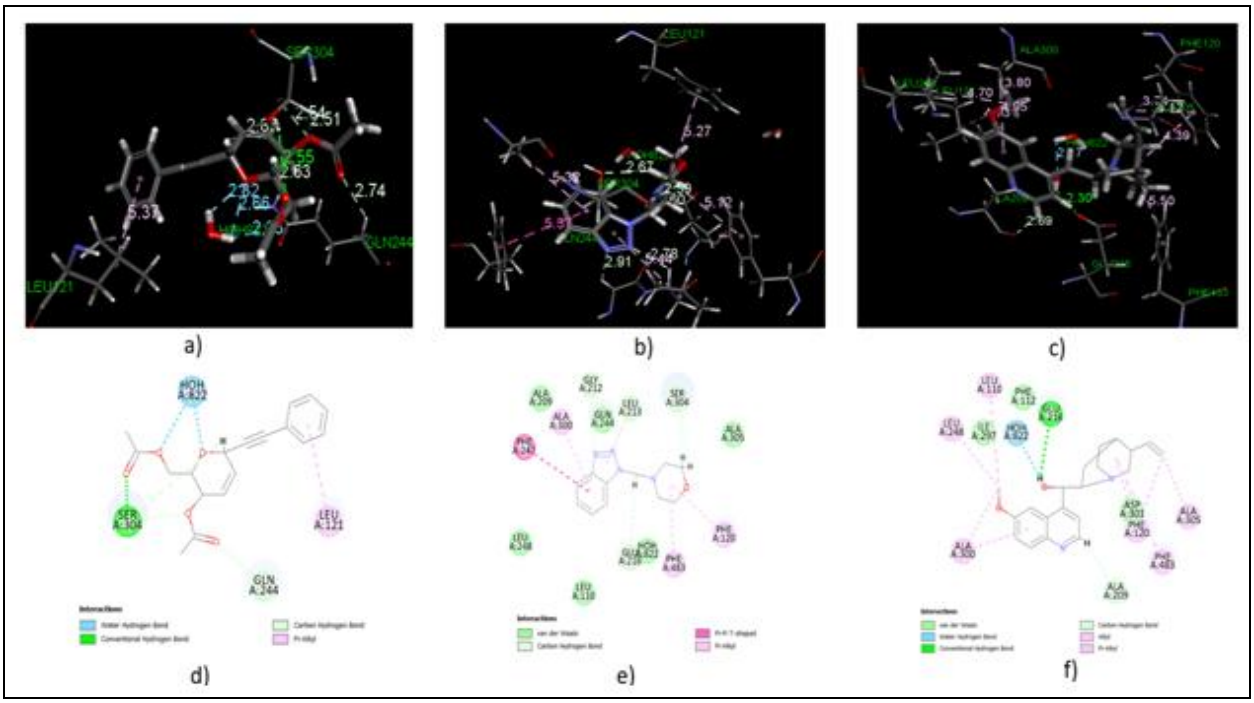

FIG. 11: (A) CMP1 DOCKING POSE WITH 4WNU (B) CMP13 DOCKING POSE WITH 4WNU (C) QUINIDINE DOCKING POSE WITH 4WNU (D) CMP1 INTERACTION DIAGRAM WITH 4WNU E) CMP13 INTERACTION DIAGRAM WITH 4WNU (F) QUINIDINE INTERACTION DIAGRAM WITH 4WNU

TABLE 4: DOCKING RESULTS OF COMPOUNDS CMP1, CMP13 AND QUINIDINE WITH 4XRZ

S. no.	Compound	-CDOCKER Energy	-CDOCKER Interaction Energy
1	cmp1	23.5713	40.691
2	cmp13	12.6244	29.6301
3	quinidine	-12.0632	45.9235

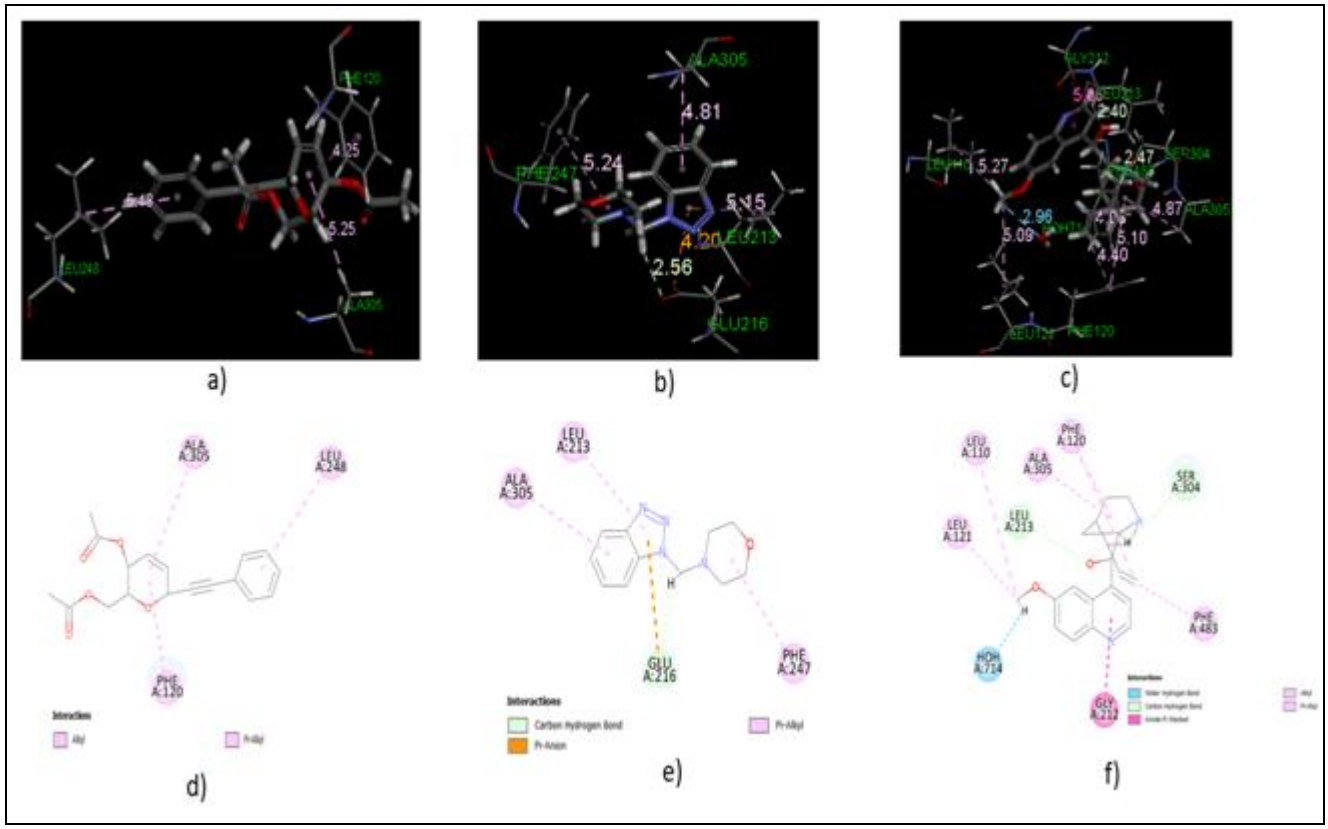

FIG. 12: (A) CMP1 DOCKING POSE WITH 4XRZ (B) CMP13 DOCKING POSE WITH 4XRZ (C) QUINIDINE DOCKING POSE WITH 4XRZ D) CMP1 INTERACTION DIAGRAM WITH 4XRZ (E) CMP13 INTERACTION DIAGRAM WITH 4XRZ (F) QUINIDINE INTERACTION DIAGRAM WITH 4XRZ

DFT Calculations: Using the density functional quantum mechanics method in DMol3, the Calculate Energy (DFT) protocol allowed us to determine the energy or optimize the shape of a group of tiny molecules. Characteristics including the dipole, atomic charges, HOMO and LUMO energies, and total energy, among others. This protocol helped to perform density functional QM calculation using DMol3. It used density functional theory (DFT), which is implemented in DMol3, to calculate a range of molecular and atomic characteristics. Using delocalized internal coordinates, DMol3 has long been one of the quickest techniques for molecular DFT computations and can efficiently carry out structure optimizations of molecular systems. The protocol has calculated various energies such as total energy, binding energy, HOMO and LUMO energy and dipole magnitude. The electron density isovalue is set to 0.03 by default. Molecular orbitals have two phases: the positive phase, which is coloured blue, has an isovalue of 0.01 and is colored negatively, which is colored red. In Figure 13, a comprehensive pictorial representation is provided. In **Fig. 13A**, the electrostatic potential is mapped on the isosurface of the electron density of cmp1, and in **Fig. 13B**, the electrostatic potential is mapped on the isosurface of the electron density of cmp13. **Fig. 13C** displays the visualization of the HOMO molecular orbitals of cmp1, while **Fig. 13D** displays the visualization of the HOMO molecular orbitals of cmp13. **Fig. 13E** describes the LUMO molecular orbitals of cmp1 and **Fig. 13F** displays the LUMO molecular orbitals of cmp13. However, **Table 5** has displayed all the energies calculated with the implementation of DMol3, the total energy of cmp1 is -1,063.33 and cmp13 is -715.506, the binding energy of cmp1 is -7.83124 and for cmp13 is -5.7123, HOMO and LUMO energies for cmp1 were found to be -0.198091 and -0.105304,

whereas for cmp13 HUMO was found to be -0.186289 and LUMO -0.0798764. The dipole magnitude calculated for both cmp1 and cmp13 was 2.58611 and 1.98999 respectively.

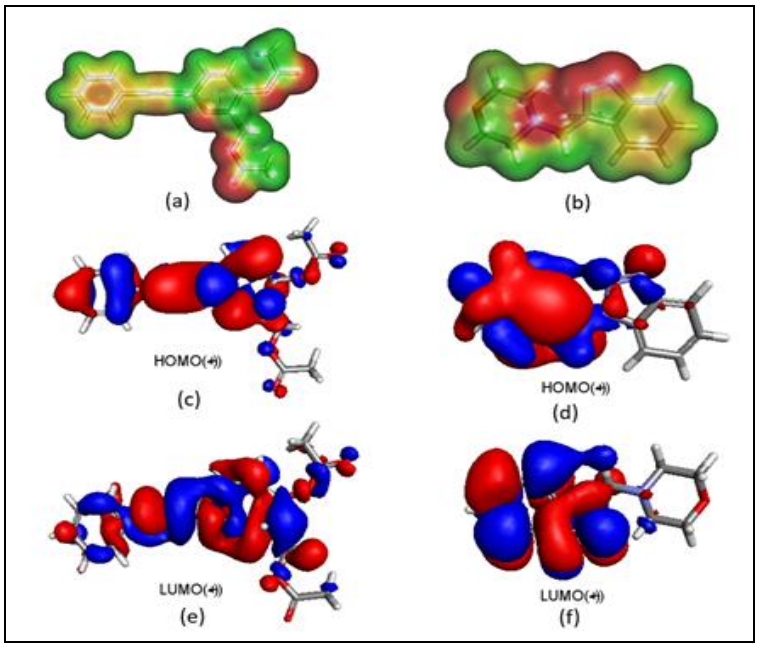

FIG. 13: (A) SURFACE PLOTS SHOWING THE ELECTROSTATIC POTENTIAL MAPPED ON THE ISOSURFACE OF THE ELECTRON DENSITY OF CMP1 (B) SURFACE PLOTS SHOWING THE ELECTROSTATIC POTENTIAL MAPPED ON THE ISOSURFACE OF THE ELECTRON DENSITY OF CMP13 (C) VISUALIZATION OF THE HOMO MOLECULAR ORBITALS OF CMP1 (D) VISUALIZATION OF THE HOMO MOLECULAR ORBITALS OF CMP13 (E) VISUALIZATION OF THE LUMO MOLECULAR ORBITALS OF CMP1 (F) VISUALIZATION OF THE LUMO MOLECULAR ORBITALS OF CMP13

TABLE 5: DETAILS OF CALCULATED MOLECULAR PROPERTIES OF CMP1 AND CMP2

S. no.	Compound	Total_energy_ DMol3	Binding_energy_D Mol3	HOMO_energy_D Mol3	LUMO_Energy_ DMol3	Dipole_Mag_ DMol3
1	cmp1	-1,063.33	-7.83124	-0.198091	-0.105304	2.58611
2	cmp13	-715.506	-5.7123	-0.186289	-0.0798764	1.98999

Molecular Dynamic Simulation: An understanding of the biomolecule's atomic structure is extremely beneficial and frequently yields significant insight into how it functions. However, because the atoms in a biomolecule are constantly in motion, the dynamics of the individual molecules affect both their intramolecular connections and molecular function. In addition to a static image, it would be appealing to be able to view these biomolecules in motion, tamper with them at the atomic level, and observe how they react. Unfortunately, controlling how individual atoms move while being observed is challenging. Working with a computer simulation of the relevant proteins at the atomic level is an appealing alternative. Based on a broad model of the physics driving interatomic interactions, molecular dynamics (MD) simulations predict the long-term motion of every atom in a protein or other molecular system [51]. Molecular dynamics can be used to generate a realistic model of a structure's motion, perform conformational searching, produce a time series analysis of structural and energetic properties, explore energy decay, and analyze solvent effects. Molecular dynamics simulations may help in understanding critical aspects of protein function that involve both small-scale and large-scale atomic movements. Assigning a force field to the input molecule in molecular mechanics simulations is a crucial step. On basis of our docking results, we have taken the cmp1 in complex with 4WNU for simulation studies. In the Biovia Discovery Studio, the CHARMm force field, using automatic parameter estimation allows for the systematic assignment of all forcefield parameters for virtually any form of molecule, even by inexperienced users. The CHARMm force field is a highly flexible molecular mechanics and dynamics program. After assigning the force field to the complex structure of cmp1 with 4WNU,

further subjected to solvation protocol. Where water boundaries were assigned around the complexes. This step added orthorhombic explicit solvation boundary with a minimum of 3 A˚ distance with an addition of 5171 water, 14 Sodium, 16 Chloride. Following solvation, the complexes were subjected to Standard Dynamic Cascade (SDC) protocol with two-step minimizations with maximum steps of 500 each. First, the Steepest Decent method of minimization was set followed by the Conjugate Gradient. The heating step was set to be 50ps and results were saved at each 20ps interval, targeted 300 (K) followed by 150ps equilibration. The final frames were got in the production step at 50ps with NPT type. The SDC protocol of Discovery Studio uses Leapfrog Verlet dynamic integrator with the SHAKE constraint algorithm. The restart files from SDC were subjected to Dynamics (NAMD) for 100 ns with GPU mode to get the final confirmations. The Dynamics (NAMD) of Discovery Studio uses the Langevin Dynamics algorithm for temperature control and the Langevin Piston algorithm for pressure control. The total energy, potential energy, kinetic energy, Van der Walls energy, and electrostatic energy of the system were found to be -60141.8950 kcal/mol, -75046.1817 kcal/mol, 14904.2867 kcal/mol, -421.4725kcal/mol and -81251.4142 kcal/mol respectively. The structural characteristics of a molecular dynamics trajectory can be examined using the Analyze Trajectory protocol to get the RMSD, RMSF and Rg keeping the first frame as a reference with respect to their atom fit, from backbone to backbone.

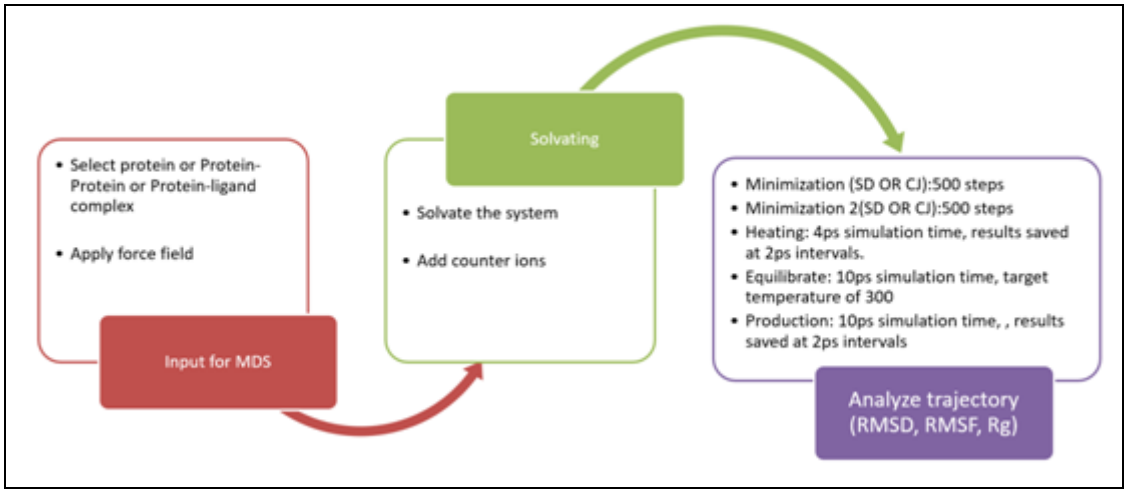

FIG. 14: FLOWCHART OF THE STEPS FOLLOWED DURING MOLECULAR DYNAMIC SIMULATION

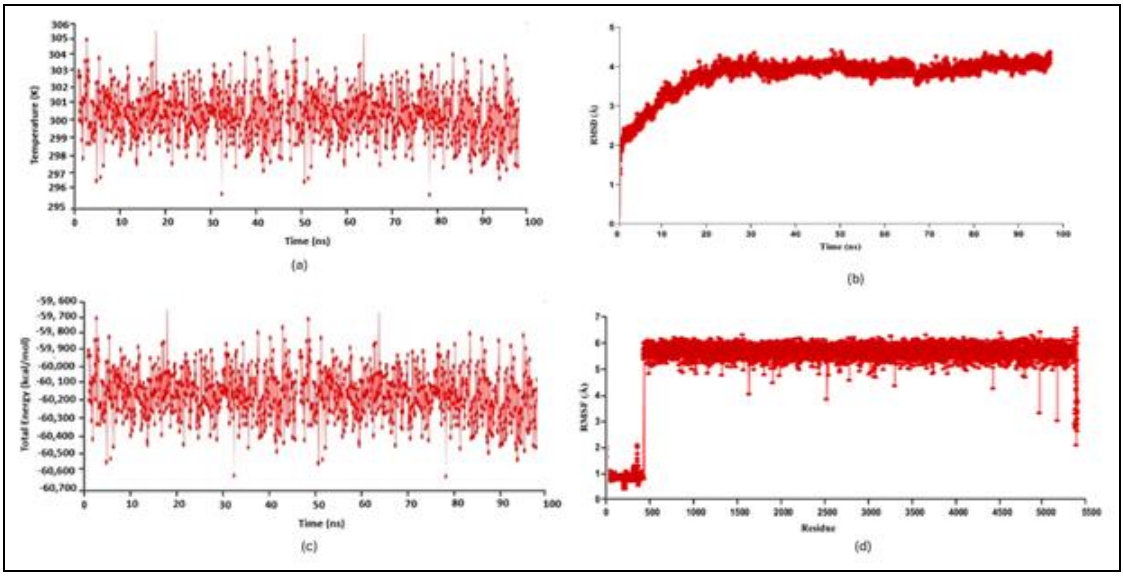

FIG. 15: (A) THE PLOT IN-BETWEEN TIME (NS) AND TEMPERATURE (K) FOR CMP1 COMPLEX WITH 4WNU (B) RMSD PLOT OF CMP1 COMPLEX WITH 4WNU (C) THE PLOT IN-BETWEEN TIME (NS) AND TOTAL ENERGY (KCAL/MOL) FOR CMP1 WITH 4WNU(D) RMSF PLOT OF CMP1 WITH 4WNU

Where the Root mean square deviation (RMSD) was studied to analyze the average movement of atoms throughout molecular dynamics simulation, Root mean square fluctuation (RMSF) was studied to analyze the fluctuation of amino acid residues / Secondary structure of protein with respective to initial structure, and Radius of gyration (Rg) was used to study weighted-RMSD of atoms as a function of time and make to ensure the compactness of the protein structure during dynamics.

MMPBSA Calculation: In drug development initiatives, it is crucial to comprehend and measure the intensity of interactions between ligands and proteins to determine how modifications to a ligand may affect binding affinity. Molecular Mechanics Generalized Born Surface Area (MM-GBSA) was used to calculate the binding free energy change of the simulated trajectories, utilizing vander Wall atomic radii and an implicit solvent dielectric constant of 80. Using the Momany Rone partial charge estimation method, the entropy temperature was maintained at 298.15 kelvin as the default value. TheMMPBSA was calculated as DeltaG_Average -26.1570 kcal/mol.

CONCLUSION: In the present work, we have taken the series of 2815 small molecules which are present in the 3D databases of Biovia Discovery studio 2022 against Cytochrome P450 2D6 *via in-silico* screening. By applying pharmacokinetic and pharmacodynamic filters for high throughput screening we have got 25 molecules from the series. Whereas two compounds cmp1 and cmp13have shown capabilities against these filters, so we have taken these two molecules for molecular docking and molecular dynamic simulations studies to check their binding interactions, affinity and sustainability. The docking studies have revealed that the compound cmp1in complex with 4WNU had exhibited the lowest -CDOCKER energy and -CDOCKER interaction energy with values 26.4705 kcal/mol and 44.37 kcal/mol respectively, whereas cmp13 exhibited the -CDOCKER energy and -CDOCKER interaction energy with values 14.9831 kcal/mol and 31.9318 kcal/mol respectively. The docking studies of cmp1 and amp13 with 4XRZ demonstrated that cmp1 exhibited -CDOCKER energy and -CDOCKER interaction energy with values of 23.5713 kcal/mol and 40.691 kcal/mol respectively, whereas cmp13 exhibited 12.6244 kcal/mol and 29.6301 kcal/mol respectively. The standard molecule i.e. quinidine, has shown -17.8009 kcal/mol and 44.2938 kcal/mol as -CDOCKER energy and -CDOCKER interaction energy with 4WNU and -12.0632 kcal/mol 45.9235 kcal/mol as -CDOCKER energy and -CDOCKER interaction energy with 4XRZ. Based on these results, we have taken compound cmp1 for our molecular dynamic simulations to check the sustainability and stability of cmp1 in a complex with 4WNU. The CHARMms-based molecular dynamic simulation was employed for 100 ns. The RMSD was RMSF recorded with respect to the backbone-to-backbone atom group fit for each conformation. The MMPBSA binding energies were also calculated. The molecular visualization revealed that cmp1 as an inhibitor for 4WNU showed significant binding. Hence, we have considered cmp1 as a potential molecule based on computational analysis including molecular docking and molecular dynamic simulations. As we have concluded that cmp1 has shown interestingly significant results with 4WNU than 4XRZ. The present study, based on computational analysis has demonstrated that cmp1 has great potential as a Cytochrome P450 2D6 inhibitor. In order to demonstrate the same, this molecule needed to be further examined *in-vitro* and *in-vivo*.

ACKNOWLEDGEMENT: The authors are grateful to Altem Technologies, Bengaluru, India, for their support in conducting the research work.

CONFLICTS OF INTEREST: Nil

REFERENCES:

1. Nebert DW: Pharmacogenetics and pharmacogenomics: why is this relevant to the clinical geneticist? Clinical Genetics 1999; 56: 345–347.
2. Arshad S, Butt J, Ahmed R and Ijaz M: Pharmacogenetics, mini-review. Journal of Analytical & Pharmaceutical Research 2018; 7: 147–50.
3. Bank PCD, Caudle KE, Swen JJ, Gammal RS, Whirl-Carrillo M and Klein TE: Comparison of the guidelines of the clinical pharmacogenetics implementation consortium and the dutch pharmacogenetics working group. Clinical Pharmacology and Therapeutics 2018; 103:599–618.
4. Ann KD: Pharmacogenetics: a general review on progress to date. British Medical Bulletin 2017; 124: 65–79.
5. Ingelman-Sundberg M, Sim SC, Gomez A and Rodriguez-Antona C: Influence of cytochrome P450 polymorphisms on drug therapies: pharmacogenetic, pharmacoepigenetic

and clinical aspects Pharmacology & Therapeutics 2007; 116: 496–526.
6. Rendic S and Guengerich FP: Contributions of human enzymes in carcinogen metabolism. Chemical Research in Toxicology 2012; 25: 1316–1383.
7. Blackburn HL, Ellsworth DL, Shriver CD and Ellsworth RE: Role of cytochrome P450 genes in breast cancer etiology and treatment: effects on estrogen biosynthesis, metabolism, and response to endocrine therapy. Cancer Causes Control 2015; 26: 319–332.
8. Gardiner SJ and Begg EJ: Pharmacogenetics, drug-metabolizing enzymes, and clinical practice. Pharmacological Reviews 2006; 58: 521–590.
9. Gaedigk A, Sangkuhl K, Whirl-Carrillo M, Klein T and Steven LJ: Prediction of CYP2D6 phenotype from genotype across world populations. Genetics in Medicine 2017; 19: 69–76.
10. Leppert W: CYP2D6 in the metabolism of opioids for mild to moderate pain. Pharmacology 2011; 87: 274–285.
11. WangBo, Li-Ping Y, Xiao-Zhuang Z, Shui-Qing H, Mark B & Shu-Feng Z: New insights into the structural characteristics and functional relevance of the human cytochrome P450 2D6 enzyme. Drug Metabolism Reviews 2009; 41: 573-643.
12. Puangpetch A, Vanwong N, Nuntamool N, Hongkaew Y, Chamnanphon M and Sukasem M: CYP2D6 polymorphisms and their influence on risperidone treatment. Pharmacogenomics and Personalized Medicine 2016; 1: 131-147.
13. Wang D, Poi MJ, Sun X, Gaedigk A, Leeder JS and Sadee W: Common CYP2D6 polymorphisms affecting alternative splicing and transcription: long-range haplotypes with two regulatory variants modulate CYP2D6 activity. Human Molecular Genetics 2014; 1: 268-78.
14. Matthew AB, Edwards S, Hoyle E, Campbell S, Laval S, Daly AK, Pile KD, Calin A, Ebringer A and Weeks DE: Wordsworth, B.P.Polymorphisms of the CYP2D6 gene increase susceptibility to ankylosing spondylitis. Human Molecular Genetics 2000; 9: 1563–1566.
15. Zanger UM and Schwab M: Cytochrome P450 enzymes in drug metabolism: Regulation of gene expression, enzyme activities, and impact of genetic variation. Pharmacology & Therapeutics 2013; 138: 103-141.
16. Sadee W, Wang D, Papp AC, Pinsonneault JK, Smith RM and Moyer RA: Pharmacogenomics of the RNA world: structural RNA polymorphisms in drug therapy. Clinical Pharmacology and Therapeutics 2011; 89: 355-365.
17. Meyer UA: Pharmacogenetics — five decades of therapeutic lessons from genetic diversity. Nature Reviews Genetics 2004; 5: 669-676.
18. Shu-Feng Z, Jun-Ping L & Balram C: Polymorphism of human cytochrome P450 enzymes and its clinical impact. Drug Metabolism Reviews 2009; 41: 89-295.
19. Ingelman-Sundberg M: Human drug metabolising cytochrome P450 enzymes: properties and polymorphisms. Naunyn-Schmiedeber Arch of Pharma 2004; 369: 89–104.
20. Preissner SC, Hoffmann MF, Preissner R, Dunkel M, Gewiess A and Preissner S: Polymorphic Cytochrome P450 Enzymes (CYPs) and Their Role in Personalized Therapy. PLoS ONE 2013; 8: e82562.
21. Zhou SF, Liu JP, Chowbay B: Polymorphism of human cytochrome P450 enzymes and its clinical impact. Drug Metabolism Reviews 2009; 41: 89-295.
22. Ramachandran GN, Ramakrishnan C and Sasisekharan V: Stereochemistry of polypeptide chain configurations. Journal of Molecular Biology 1963; 7: 95.
23. McGraw J and Waller D: Cytochrome P450 variations in different ethnic populations. Expert Opinion on Drug Metabolism & Toxicology 2012; 8: 371-382.
24. Spatzenegger M & Jaeger W: Clinical importance of hepatic cytochrome P450 in drug metabolism. Drug Metabolism Reviews 1995; 27: 397-417.
25. Ogu CC & Maxa JL: Drug Interactions Due to Cytochrome P450, Baylor University Medical Center Proceedings 2000; 13: 421-423.
26. BIOVIA, Dassault Systèmes, [Discovery Studio], [2022], San Diego: Dassault Systèmes 2022.
27. Prabhakaran P, Prashantha BRK, Shanmugarajan D & Suresh B: Curcumin to inhibit binding of spike glycoprotein to ACE2 receptors computational modelling, simulations, and ADMET studies to explore curcuminoids against novel SARS-CoV-2 targets. RSC Advances 2020; 10: 31385-31399.
28. Kerns D and LiDi: Drug-like Properties: Concepts, Structure Design and Methods: from ADME to Toxicity Optimization. Academic Press 2008; 1-549.
29. William JE and Lauri G: Prediction of intestinal permeability. Advanced Drug Delivery Reviews 2002; 54: 273-289.
30. Cheng A and Dixon SL: *In-silico* models for the prediction of dose-dependent human hepatotoxicity. Journal of Computer-Aided Molecular Design 2003; 17: 811-823.
31. Egan WJ, Merz KM and Baldwin JJ: Prediction of drug absorption using multivariate statistics. Journal of Medicinal Chemistry 2000; 43: 3867-3877.
32. Cheng A and Merz KM: Prediction of aqueous solubility of a diverse set of compounds using quantitative structure-property relationships. Journal of Medicinal Chemistry 2003; 46: 3572-3580.
33. Dixon SL and Merz KM: One-dimensional molecular representations, and similarity calculations: methodology and validation. Journal of Medicinal Chemistry 2001; 44: 3795-809.
34. Votano JR, Parham M, HallLM, Hall LH, Kier L and Oloff S, Tropsha A: QSAR Modeling of Human Serum Protein Binding with Several Modeling Techniques Utilizing Structure-Information Representation. Journal of Medicinal Chemistry 2006; 49: 7169-7181.
35. Leach AG, Jones HD, Cosgrove DA, Kenny PW, Ruston L, MacFaul P, Wood JM, Colclough N, Law B: Matched molecular pairs as a guide in the optimization of pharmaceutical properties; a study of aqueous solubility, plasma protein binding and oral exposure. Journal of Medicinal Chemistry 2006; 49: 6672-6682.
36. Egan WJ and Lauri G: Prediction of molecular polar surface area and bioabsorption. U.S. Patent 2006; US7113870 B2.
37. Kazius J, McGuire R and Bursi R: Derivation and validation of toxicophores for mutagenicity prediction. Journal of Medicinal Chemistry 2005; 48: 312-320.
38. Contrera JF, Matthews EJ, Kruhlak NL and Benz RD: *In-silico* screening of chemicals for bacterial mutagenicity using electrotopologicale-state indices and MDL QSAR Software. Regulatory Toxicology and Pharmacology 2005; 43:313-323.
39. Ashby J and Tennant RW: Chemical structure, salmonella mutagenicity and extent of carcinogenicity as indicators of genotoxic carcinogenesis among 222 chemicals tested in Rodents by the U.S. NCI/NTP Mutation Research 1988; 204: 17-115.
40. Politzer P and Seminario JM: Eds. Density Functional Theory: A Tool for Chemistry, Elsevier: Amsterdam, 1995.

41. Weinshilboum R: Inheritance and drug response. The New England Journal of Medicine 2003; 348: 529–537.
42. Wang A, Stout CD, Zhang Q and Johnson EF: Contribution of ionic interactions as protein dynamics to cytochrome P4502D6 (CYP2D6) substrate and inhibitor. Binding Journal of Biological Chemistry 2015; 290: 5092-5104.
43. Brodney MA, Beck EM, Butler CR, Barreiro G, Johnson EF and Riddell D: Utilizing Structures of CYP2D6 and BACE1 Complexes To Reduce Risk of Drug-Drug Interactions with a Novel Series of Centrally Efficacious BACE1 Inhibitors. J of Med Chemis 2015; 58: 3223–52.
44. An J, Totrov M and Abagyan R: Pocketome *via* comprehensive identification and classification of ligand binding envelopes. Molecular & Cellular Proteomics 2005; 4: 752–61.
45. Laurie AT and Jackson RM: Q-site finder: an energy-based method for the prediction of protein–ligand binding sites. Bioinformatics 2005; 21: 1908–16.
46. Yu W, Lakkaraju S, Raman EP and Alexander MJD: Site-identification by ligand competitive saturation (silcs) assisted pharmacophore modelling. Journal of Computer-Aided Molecular Design 2014; 28: 491–507.
47. Wu G, Robertson DH, Brooks CLIII and Vieth M: Detailed analysis of grid-based molecular docking: A case study of CDOCKER- A CHARMm-based MD docking algorithm. Journal of Computational Chemistry 2003; 2: 1549.
48. Tirado-Rives J and Jorgensen WL: Contribution of conformer focusing on the uncertainty in predicting free energies for protein-ligand binding. Journal of Medicinal Chemistry 2006; 49: 5880-5884.
49. Gallicchio E and Levy RM: AGBNP: an analytic implicit solvent model suitable for molecular dynamics simulations and high-resolution modelling. Journal of Computational Chemistry 2004; 25: 479-499.
50. Justin A,Mandal S, Prabitha P, Dhivya S, Yuvaraj S, Kabadi P and Sekhar SJ: Rational design, synthesis, and in vitro neuroprotective evaluation of novel glitazones for PGC-1α activation *via* PPAR-γ: a new therapeutic strategy for neurodegenerative disorders, Neurotoxicity Research 2019; 1-17.
51. Karplus M and McCammon JA: Molecular dynamics simulations of biomolecules. Nature Structural & Molecular Biology 2002; 9: 646–652.

How to cite this article:
Bhardwaj S and Shanmugarajan D: Computational exploration of small molecules as inhibitor targetting cytochrome p4502d6. Int J Pharm Sci & Res 2024; 15(9): 2755-72. doi: 10.13040/IJPSR.0975-8232.15(9).2755-72.